Retarded long-range interaction in split-ring-resonator square arrays

Manuel Decker,[1,2] Nils Feth,[1,2] Costas M. Soukoulis,[3,4] Stefan Linden,[1,2,5] and Martin Wegener[1,2]

[1]*Institut für Nanotechnologie, Karlsruhe Institute of Technology (KIT), Hermann-von-Helmholtz-Platz 1,*
D-76344 Eggenstein-Leopoldshafen, Germany

[2]*Institut für Angewandte Physik and DFG-Center for Functional Nanostructures (CFN), Karlsruhe Institute of Technology (KIT),*
Wolfgang-Gaede Strasse 1, D-76131 Karlsruhe, Germany

[3]*Ames Laboratory and Department of Physics and Astronomy, Iowa State University, Ames, Iowa 50011, USA*

[4]*IESL-FORTH and Department of Materials Science and Technology, University of Crete, GR-71110 Heraklion, Greece*

[5]*Physikalisches Institut, Universität Bonn, Nußallee 12, D-53115 Bonn, Germany*

We systematically investigate the optical extinction spectra of planar gold split-ring-resonator square arrays operating at ~200-THz frequency versus the lattice constant and versus angle of incidence. We find a strong dependence of the resonance damping on the in-plane wave vector, namely, the resonance damping increases (decreases) versus the in-plane wave vector for small lattice constants (large lattice constants). By comparison with two simple one-dimensional models as well as with more complete numerical calculations, this behavior is interpreted in terms of a long-range retarded interaction among the split-ring resonators. In contrast, the assumptions of only nearest-neighbor interaction and/or of an instantaneous interaction lead to a striking disagreement with the overall experimental facts.

I. INTRODUCTION

Split-ring resonators[1–5] are tiny subwavelength electromagnets into which an incident electromagnetic light field can induce a circulating and oscillating electric current, leading to a local magnetic-dipole moment normal to the plane of the ring. Split-ring resonators (SRRs) are the paradigm building block (or "meta-atom") of metallic metamaterials[3] and can be viewed as the classical counterpart of quantum-mechanical magnetic moments due to spin or atomic-orbital angular moments.[6]

For many applications, it is desirable to achieve a small damping (or linewidth) of the SRR resonance. Thus, a detailed understanding of the mechanisms determining this linewidth is highly desirable. It is well known by now that both near-field as well as far-field coupling effects significantly modify the resonance position and line shape of the response of coupled metal nanoparticles.[7–10] Likewise, for SRR arrays the damping is not only determined by the properties of the individual SRRs but also by the mutual interaction of SRRs in a two-dimensional array[5,6,11] or in a three-dimensional crystal.[12–15] This fact was already reported in our early SRR experiments[3] at 100-THz frequency in 2004, where we observed that the magnetic-resonance damping varies significantly with lattice constant. In 2009, this behavior was interpreted in terms of superradiance for usual SRR square arrays investigated for several lattice constants but only under normal incidence of light.[11] We have rather interpreted our own angle-resolved experiments on particular asymmetric SRR arrays in terms of far-field retardation effects[6] which basically yield the analog of usual quantum-mechanical magnon waves in solids, with the subtle and important difference that the back action from one classical SRR to its neighbors happens with a certain time delay due to the finite SRR spacing as compared to the wavelength of light—the quantum-mechanical spin-spin interaction, on the other hand, is an example of a practically instantaneous process. As a result, the effective damping of a SRR array depends on both the lattice constant of the

SRR array and the relative phase with which the individual SRRs oscillate, hence, the excitation angle. The latter point is equivalent to saying that the damping depends on the in-plane wave vector of the excitation as the parallel (or in-plane) component of the incident wave vector of light with respect to the SRR-array plane is conserved. This dependence of the SRR damping on in-plane wave vector is precisely what we observed in our experiments.[6] However, these experiments were performed on highly unusual asymmetric SRR arrays with two nonequivalent SRRs in the primitive unit cell. Hence it remained unclear whether our interpretation would also apply for usual SRR square arrays that are much more relevant in the context of metamaterials.

In this paper we present the corresponding experimental results for the usual square arrays of SRRs for different lattice constants and excitation angles. The quality and completeness of these data go far beyond previous angle-resolved work on SRR arrays by us at optical frequencies[16] and by others at microwave frequencies[17,18] that would not have allowed for any of the conclusions of the present paper.

II. EXPERIMENTAL RESULTS

The SRR arrays in our experiments have been fabricated by standard electron-beam lithography on glass substrates coated with a 5-nm thin film of indium-tin oxide followed by standard high-vacuum electron-beam evaporation and a lift-off procedure.[3] The gold-film thickness is 40 nm and the footprint of all arrays is 160 μm × 160 μm. The normal-incidence fundamental SRR resonance is located at ~200-THz frequency (or 1500-nm free-space wavelength). The square lattice constant a of the SRR arrays is systematically varied from 280 to 700 nm. Selected typical electron micrographs are depicted in Fig. 1. Transferring these lattice constants to corresponding free-space phase delays φ we obtain values ranging from 67° to 168° between two lattice sites. In bulk glass with a refractive index of 1.4 (hence ~1071-nm material
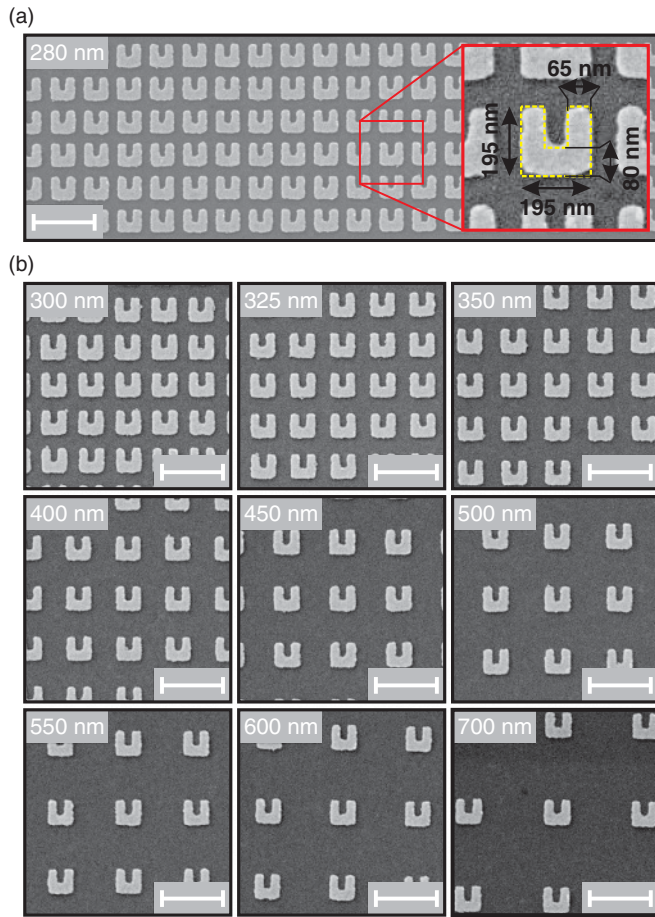
(a)

(b)

FIG. 1. (Color online) (a) Overview electron micrograph of the split-ring-resonator (SRR) square array with $a = 280$ nm lattice constant used in this paper. The total footprint of this array and all others is $160\,\mu$m $\times$ $160\,\mu$m. The SRR dimensions used for the numerical calculations are indicated in the inset. (b) Electron micrographs of all other SRR arrays in this work with lattice constants a as indicated. All arrays are shown on the same scale—the scale bar is 500 nm.

wavelength), they would correspond to phase delays ranging from 94° to 235°. Since the SRR arrays are processed on a glass half-space in air, the actual phase delays are expected to lie somewhere in between these values. Notably, we expect that we pass a phase delay of $\varphi = 180°$ at some lattice constant between 280 and 700 nm. For measurement of the intensity transmittance of the SRR arrays we use a homebuilt spectroscopy setup and an optical spectrum analyzer. Under normal-incidence conditions, the opening angle of the incident light is 5° and the imaged sample area is a square with $50\,\mu$m $\times$ $50\,\mu$m. The size increases to $100\,\mu$m along the y direction at $\beta = 60°$ (see the geometry depicted in Fig. 2). This value is still sufficiently smaller than the sample size of $160\,\mu$m (see above), avoiding artifacts from insufficient sample-spot overlap. However, at yet larger angles, the absence of artifacts can no longer be guaranteed. Thus, we limit the experiments to a maximum angle of $\beta = 60°$. The incident electric-field vector is chosen to be parallel to the SRR gap and the transmittance spectra are measured as a function of the angle of incidence for s polarization of light. The
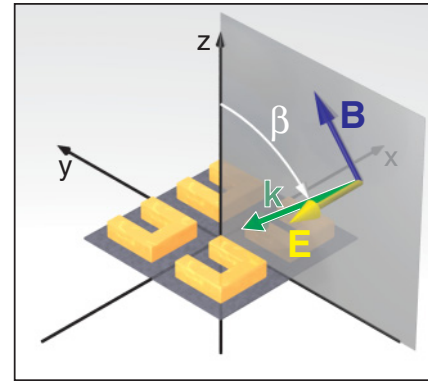

FIG. 2. (Color online) Illustration of the geometry used in our oblique-incidence optical transmittance experiments.

transmitted spectrum is normalized to the transmission of the bare glass substrate right next to the SRR arrays at the same angle of incidence in order to allow for reproducible and reliably calibrated results. We calculate the extinction spectrum defined as the negative logarithm of the measured transmittance $[-\log_{10}(T)]$.

All measured extinction spectra could very nicely be fitted by Lorentzian line shapes as illustrated in Fig. 3. These high-quality fits to high-quality raw data are the key to determining the dispersion of the SRR-resonance center position as well as of its damping with an error as low as 0.1 THz, which is only
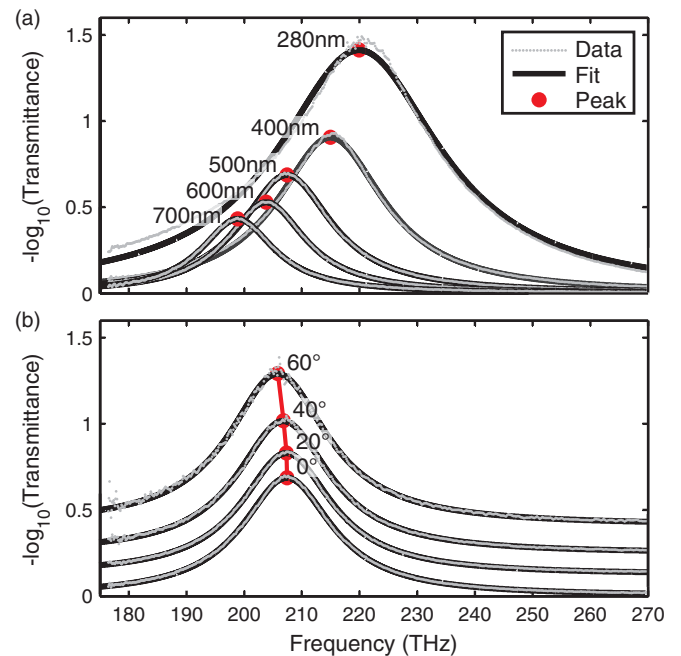

FIG. 3. (Color online) Selected extinction spectra (dots) together with Lorentzian fits (solid curves) (a) for different lattice constants at normal incidence and (b) for a selected lattice constant of $a = 500$ nm but for different angles of incidence β, as indicated. These fits provide us with the center frequency and the damping vs lattice constant and vs angle of incidence. The latter can be converted into an in-plane wave vector $k_{||}$ using the experimental geometry shown in Fig. 2. For clarity, the curves in (b) are vertically displaced by 0.1 starting with a 20° angle.

~0.05% of the resonance center frequency of 200 THz. This error has been determined by repeating the experiment and the fitting procedure. We do the experiment for SRR square arrays with lattice constants of 280, 300, 325, 350, 400, 450, 500, 550, 600, and 700 nm. The angle of incidence β with respect to the surface normal is varied from 0° to 60° in steps of 5° (i.e., $10 \times 13 = 130$ spectra altogether). Finer steps do not make sense as the opening angle of the incident light is ~5° as well. For each parameter combination we perform the Lorentzian fit and obtain the resonance center frequency and its damping (half the linewidth of the SRR resonance). The angle of incidence β is converted into an in-plane wave vector via the formula

$$k_{||} = k_0 \sin(\beta), \qquad (1)$$

with the free-space wave number $k_0 = 2\pi/\lambda$, where λ is the free-space resonance wavelength. Negative and positive angles of incidence have delivered consistent results, as verified for selected examples. Thus, in what follows, we only show results for positive angles. The corresponding experimental data are summarized in Fig. 4.

For the combination of large lattice constants with large angles of incidence, caution has to be exerted because under these conditions light can be diffracted into the glass substrate, corresponding to well-known Wood anomalies. In this case the spectra deviate from Lorentzian line shapes, leading to inaccurate results from the fitting procedure for the SRR resonance positions and linewidths. The crosses in
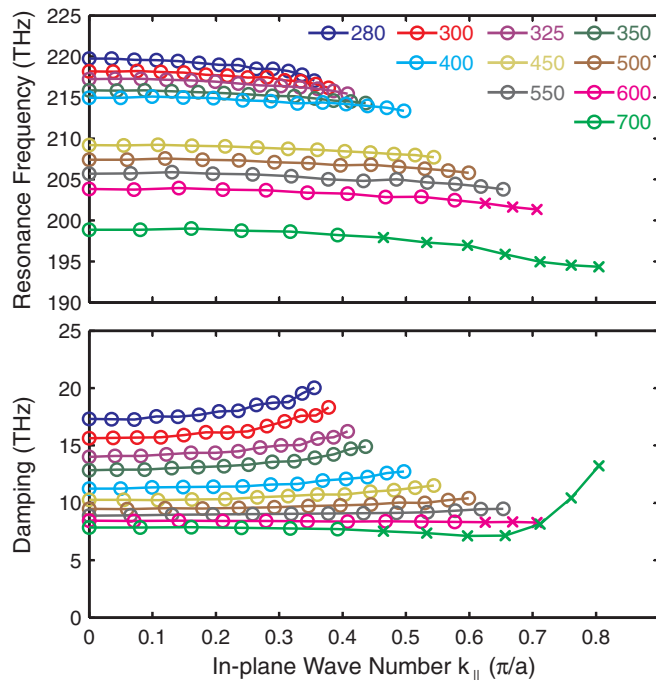

FIG. 4. (Color) Center frequency (top) and damping (bottom) vs in-plane wave vector $k_{||}$ for different lattice constants a, as indicated (in units of nm). These data are derived from Lorentzian fits to the experimental data as illustrated in Fig. 3. The crosses illustrate the data points for which the influence of diffraction into the glass substrate (Wood anomaly) may become important. These data points should be taken with some caution. All curves end at a maximum angle of incidence with respect to the surface normal of 60° (see Fig. 2).

Fig. 4 indicate the data points for which the Wood-anomaly frequency is expected to be separated from the fundamental SRR resonance frequency by less than two SRR resonance full linewidths—a very conservative estimate. In fact, only for these data points, the behavior of the damping changes qualitatively, indicating a substantial influence of the Wood anomaly onto our results. For the remaining data points in Fig. 4 we can safely conclude that the observed change in sign of the SRR resonance damping versus in-plane wave vector is not an artifact of the Wood anomaly.

In the experiments we observe a dispersion of the resonance center frequency versus the in-plane wave vector as expected for any type of interaction effect. Specifically, the resonance center frequency decreases with increasing in-plane wave vector and with increasing lattice constant. This dispersion corresponds to negative group velocities of light, i.e., to backward waves. More importantly, we find that the SRR resonance linewidth or damping increases with increasing in-plane wave vector $k_{||}$ for small lattice constants. This increase becomes less pronounced for larger lattice constants and may in itself be partly due to decreased magnitude of the SRR interaction strength. However, if the lattice constant exceeds a value of approximately $a = 600$ nm, the measured resonance damping starts decreasing (!) with increasing in-plane wave vector $k_{||}$.

This finding cannot be explained by reduced coupling strength alone and is a fingerprint for retarded interaction among the SRRs, as investigated previously in the context of asymmetric SRR arrays.[6] However, in the case investigated here, the overall qualitative behavior of the dispersion of both the resonance frequency and the damping can only be described if we account for long-range interaction effects, as we shall argue in what follows.

III. HEURISTIC COUPLED-OSCILLATOR MODEL

Let us start by comparing the experimental findings to a very simple but intuitive one-dimensional toy model that we have previously introduced for the case of nearest-neighbor interactions only.[6] The model considers an infinite one-dimensional chain of harmonic oscillators with individual center frequency Ω and individual damping γ that are coupled to their nearest neighbors by the interaction frequency W. The latter clearly depends on the lattice constant a. The finite lattice constant a between the oscillators also leads to a time delay in their interaction, which can be translated into a phase delay φ, which is expected to be proportional to the lattice constant a. The resulting model dispersion relation for the system's complex-valued eigenfrequency ω versus real-valued in-plane wave vector $k_{||}$ is given by[6]

$$\mathrm{Re}(\omega) = +\Omega - W \cos(k_{||}a)\cos(\varphi), \qquad (2)$$

$$\mathrm{Im}(\omega) = -\gamma - W \cos(k_{||}a)\sin(\varphi). \qquad (3)$$

The real part of the eigenfrequency exhibits the usual tight-binding type dispersion, albeit modified by the cosine of the phase delay φ. More importantly, the imaginary part of the eigenfrequency, i.e., the negative resonance damping, also depends on the in-plane wave vector for nonzero values of φ. For example, for $W > 0$, the damping *decreases* with

increasing in-plane wave vector $k_{||}$ for phase delays $0° < \varphi < 180°$ because $\sin(\varphi) > 0$, whereas the damping *increases* with increasing in-plane wave vector $k_{||}$ for phase delays $180° < \varphi < 360°$, where $\sin(\varphi) < 0$. As discussed above, the phase delay is expected to be proportional to the lattice constant a. To account for the glass half-space geometry, we assume an effective refractive index of $n = 1.2$ that is intermediate to that of air and glass, in which case we obtain

$$\varphi(a) = \frac{a}{\lambda/n} 360°, \qquad (4)$$

with the free-space resonance wavelength λ obtained from the normal incidence spectra for each lattice constant.

However, we will see below that the assumption of only nearest-neighbor interaction is unable to reproduce the experimental data (Fig. 4). Following along the lines of our Ref. 6, i.e., approximating the resulting expressions in the limit of small relative frequency variations (which is well justified here—see Fig. 4), we obtain the generalized dispersion relation for interaction with all neighbors in the chain

$$\text{Re}(\omega) = +\Omega - \sum_{N=1}^{\infty} W_N \cos(Nk_{||}a)\cos(N\varphi), \qquad (5)$$

$$\text{Im}(\omega) = -\gamma - \sum_{N=1}^{\infty} W_N \cos(Nk_{||}a)\sin(N\varphi). \qquad (6)$$

Here we have used the phase delay over a distance of N lattice sites $N\varphi$. W_N is the interaction frequency with the Nth neighbor. Generally, the interaction among the SRRs is fairly complex and includes the possibility of magnetoinductive coupling[5] and magnetoelectric cross-coupling effects. The former is analogous to the coupling between the two coils of a transformer and can formally be described by magnetic dipole-dipole interaction. However, under the conditions of the above experiments, the coefficients W_N are rather expected to be dominated by electric dipole-dipole interaction.[11] This means that the interaction is governed by the decay of the electric field of an oscillating electric dipole along a direction normal to its oscillation axis. It is well known that this decay has components falling off inversely with the distance, the square of the distance, and the cube of the distance (also see the following section). In a two-dimensional array, the situation is more complex because the number of neighbors in a certain distance increases proportionally to distance. For a hypothetical isotropic interaction and an asymptotic decay of the field of one dipole with the inverse of the distance, this would lead to an effectively constant interaction, i.e., to no dependence on Na at all. However, the radiation field of an electric dipole is far from being isotropic. Hence, we expect a decay of the interaction W_N versus distance Na intermediate to a constant $\propto (Na)^0$ and $\propto (Na)^{-1}$. For simplicity, we here heuristically assume

$$W_N(a) = W_0 \sqrt{\frac{a_0}{Na}}, \qquad (7)$$

which has a rapid initial decay, followed by a long tail.

Let us start the discussion by presenting results for nearest-neighbor interaction only, i.e., we only account for the $N = 1$ contribution. Furthermore, we use the parameter
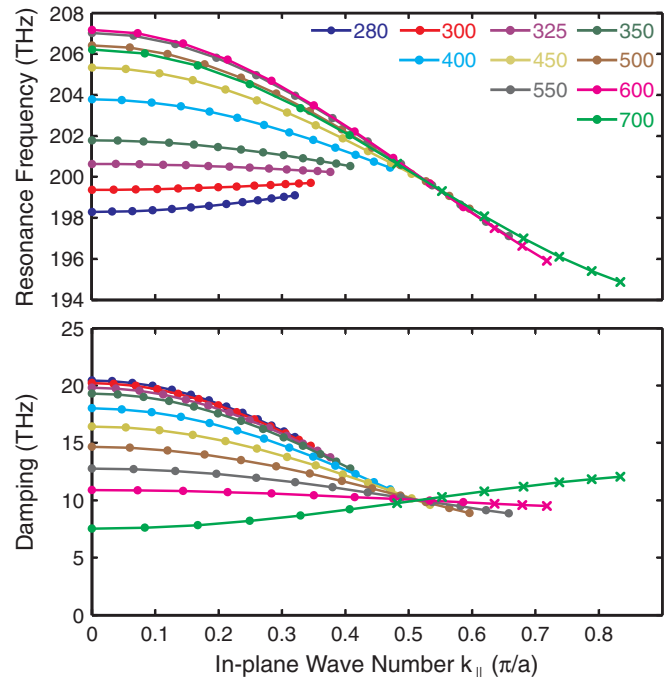

FIG. 5. (Color) Dispersion of eigenfrequency and damping as derived from a simple model of coupled harmonic oscillators subject to retarded only nearest-neighbor interaction represented as the experimental data in Fig. 4. Parameters are $\Omega/(2\pi) = 200$ THz, $\gamma/(2\pi) = 10$ THz, and $W_0\sqrt{a_0} = 66.5$ THz$\sqrt{280 \text{ nm}}$. Note the disagreement with experiment in Fig. 4. If one artificially neglects retardation (not depicted), the damping becomes strictly independent on lattice constant and strictly independent on the in-plane wave vector, i.e., the disagreement with experiment becomes even worse. Also, upon neglecting retardation, the curvature of the dispersion of the resonance frequency reverses sign, further increasing the disagreement with experiment.

$W_0\sqrt{a_0} = 66.5$ THz$\sqrt{280 \text{ nm}}$. The remaining individual-oscillator parameters are $\Omega/(2\pi) = 200$ THz and $\gamma/(2\pi) = 10$ THz. This immediately allows for calculating the resonance center frequency $\text{Re}(\omega)/(2\pi)$ and the damping $[-\text{Im}(\omega)/(2\pi)]$ versus in-plane wave vector $k_{||}$ for the various lattice constants a, just as in the experiment (Fig. 4). Results are shown in Fig. 5. Comparing the qualitative behavior of the dispersion curves, we observe that, while the behavior of the damping can be reproduced, the center-frequency dispersion is just opposite to that of the experiment. For other parameter choices, the center-frequency dispersion can be matched, however, at the price of obtaining the opposite behavior for the damping dispersion between experiment and model. What remains is a striking overall disagreement. We will see below that this disagreement also exists for more sophisticated descriptions involving only the interaction between nearest neighbors.

Next, we go beyond nearest-neighbor interaction. Results for 10 000 neighbors in each direction are depicted in Fig. 6 in the same format as the experiments in Fig. 4. Using the same set of parameters as above, we observe an improved agreement with experiment combined with a strong difference compared to the same model accounting for nearest neighbors
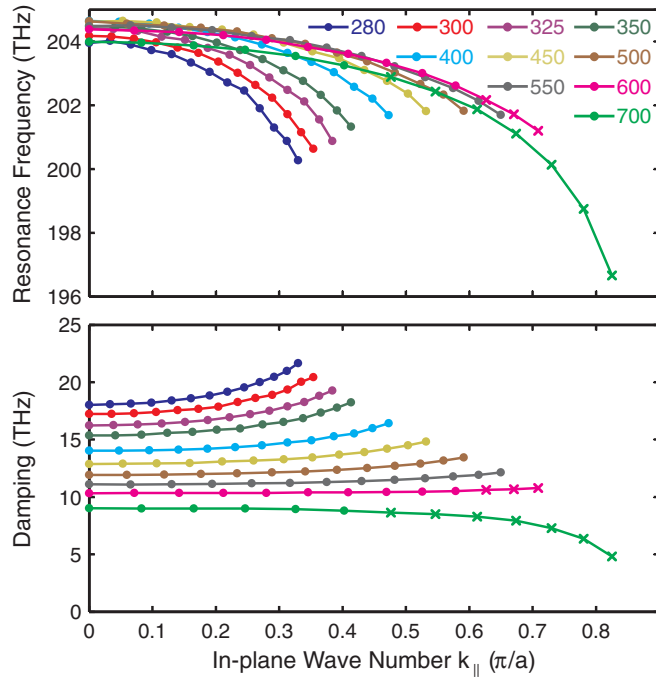
FIG. 6. (Color) As Fig. 5, but for long-range interaction between the oscillators. Parameters are chosen to be the same as for nearest-neighbor interactions only. The behavior is very much different from that of the corresponding case of nearest neighbors only in Fig. 5 and approaches that of the experiment in Fig. 4. Especially the damping is reproduced very well.

only (Fig. 5). This leads us to conclude that a retarded long-range interaction is crucial to qualitatively understand the behavior of the simple split-ring-resonator square arrays under investigation.

We note in passing that for the purely mathematical (but unphysical) case of no retardation at all (i.e., $\varphi = 0$) and zero in-plane momentum (i.e., $k_{||} = 0$), the real part of the eigenfrequency $\mathrm{Re}(\omega)$ according to (5) diverges. With retardation, no such divergence occurs, as the retardation leads to an oscillating sign of the addends in the sum via the $\cos(N\varphi)$ term.

The simple one-dimensional model of coupled harmonic oscillators applied here qualitatively explains the experimentally observed behavior. However, the model is purely heuristic. In order to back up our conclusion, we will now consider a simple but microscopic one-dimensional chain of interacting electric point dipoles (Sec. IV) in a first step. In a second step, we perform complete numerical calculations for actual two-dimensional split-ring-resonator arrays on a glass substrate (Sec. V).

IV. INTERACTING ELECTRIC POINT DIPOLES

From the geometry in Fig. 2 and from Refs. 11 and 19 it is clear that—for the in-plane wave propagation direction under consideration—the interaction among the magnetic split-ring resonators is mainly mediated via their electric-dipole moments (rather than via their magnetic-dipole moments). Thus, we will first describe this problem by a microscopic one-dimensional chain of interacting electric point dipoles—

the interaction of a set of electric dipoles has been treated many times in the literature.[20,21] For the polarizability of each isolated electric dipole α_{s}, we assume a Lorentzian response with center frequency $\Omega/(2\pi) = 200$ THz and damping $\gamma/(2\pi) = 10$ THz. Each dipole sees a total electric field composed of the monochromatic external driving field E_0 and the sum of the fields from all of the other electric dipoles E_d. Hence the effective dipole moment for this linear chain of interacting point dipoles is

$$p = \alpha_{\mathrm{s}} \left(E_0 + \sum_{d=-\infty}^{\infty} E_d \right). \tag{8}$$

Due to symmetry considerations, the sum over all dipoles $\sum_{d=-\infty}^{\infty} E_d$ can be reduced to a sum over the number of neighbors (one in each direction) $\sum_{N=1}^{\infty} \tilde{E}_N$. Using the expression for the radiation field of transversely coupled electric dipoles for the N's (two) neighbors, we obtain

$$\begin{aligned}
\tilde{E}_N &= \frac{k_0^3}{4\pi\epsilon_0} e^{ik_0 Na} \left[\frac{1}{k_0 Na} + i\left(\frac{1}{k_0 Na}\right)^2 - \left(\frac{1}{k_0 Na}\right)^3 \right] \\
&\quad \times 2\cos(k_{||}Na) \cdot p \\
&=: G_N \cdot p.
\end{aligned} \tag{9}$$

The cosine term in Eq. (9) accounts for oblique incidence of the incident light. Finally, the effective polarizability is given by

$$\alpha_{\mathrm{eff}} = \frac{\alpha_{\mathrm{s}}}{1 - \alpha_{\mathrm{s}} \sum_{N=1}^{\infty} G_N}. \tag{10}$$

The extinction is then calculated by evaluating the imaginary part of the effective polarizability α_{eff} of the linear chain of interacting dipoles. Such treatment automatically includes retardation effects, i.e., retardation does not have to be added by hand as in the above toy model. To investigate the aspect of long-range interaction, we proceed as follows. We start with one dipole and two neighbors separated by distance a in a one-dimensional setting. The resulting spectra of the imaginary part of the total system's polarizability are fitted by Lorentzians for various values of a and for various angles β just as we have proceeded with the processing of the experimental data in Sec. II.

Next, we successively increase the number of dipoles by adding more and more neighbors to the chain. Figure 7 shows the limiting case of just one neighbor in each direction and Fig. 8 that of an infinite periodic chain (actually 2001 dipoles). All other parameters have been fixed between Figs. 7 and 8. The results presented in Fig. 8 very closely qualitatively reproduce those of the simple oscillator model for long-range interaction shown in Fig. 6. This agreement provides us with further confidence that our conclusion of having observed long-range interaction effects in the experiments (Fig. 4) is indeed valid. Undoubtedly, retardation is evident by the mere fact that the damping reveals a dependence on the in-plane wave vector $k_{||}$.
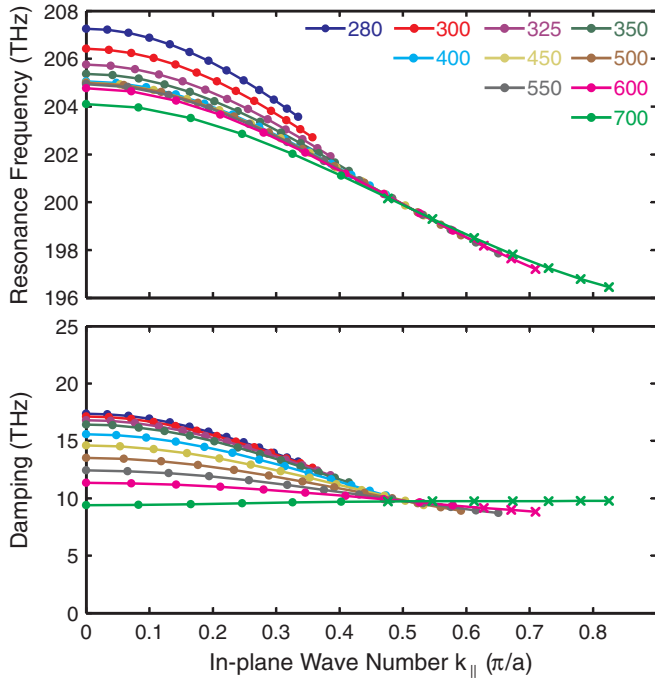
FIG. 7. (Color) Dispersion of center frequency and damping as derived from a chain of three electromagnetically interacting electric point dipoles in vacuum evenly separated by distance a, represented as the experimental data in Fig. 5. This treatment automatically accounts for retardation. The chain of three dipoles mimics short-range interaction only. Parameters are $\Omega/(2\pi) = 200$ THz and $\gamma/(2\pi) = 10$ THz. Note the disagreement with experiment in Fig. 4.
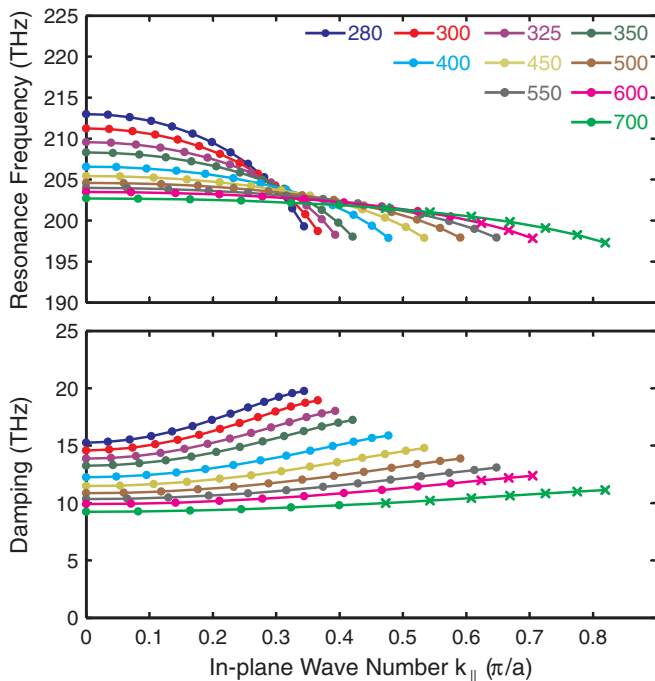
V. COMPLETE NUMERICAL CALCULATIONS

This more advanced dipole-dipole modeling has emphasized the general nature of the physics under discussion. Yet it has still not treated the particular situation of metallic split-ring resonators on a glass substrate. To this end, we have performed numerical calculations of the transmittance spectra of gold SRR arrays under oblique incidence using the commercially available program package COMSOL Multiphysics with a frequency-domain finite-elements solver and periodic boundary conditions in the SRR plane. The gold is described by a free-electron Drude dielectric function with plasma frequency $\omega_{pl} = 2\pi \times 2155$ THz and collision frequency $\omega_{coll} = 2\pi \times 28.3$ THz. The SRR array is located on a glass substrate with a refractive index of 1.41, the lattice constants are as in the experiments, the SRR thickness is 40 nm, and the lateral SRR dimensions are illustrated in Fig. 1(a). The calculated transmittance spectra are then processed just as in the experiment (Sec. II).

The results shown in Fig. 9 qualitatively agree with the experiment (Fig. 4) as well as with the simple oscillator model with long-range interaction (Fig. 6) and with the microscopic dipole-dipole description (Fig. 8). In particular, the slopes of both the eigenfrequency dispersion and the damping dispersion and their dependence on the lattice constant a are reproduced.

Caution has to be exerted when comparing the behavior of the dispersion branches of the resonance frequency for different lattice constants a. In the experiment, even variations of the SRR size of just a few percent (almost unavoidable

FIG. 8. (Color) As Fig. 7, but for 2001 rather than for three electric point dipoles. All other parameters are as in Fig. 7. Note the much better qualitative agreement with the experiment in Fig. 4 and the striking difference to the corresponding case of nearest neighbors only in Fig. 7.
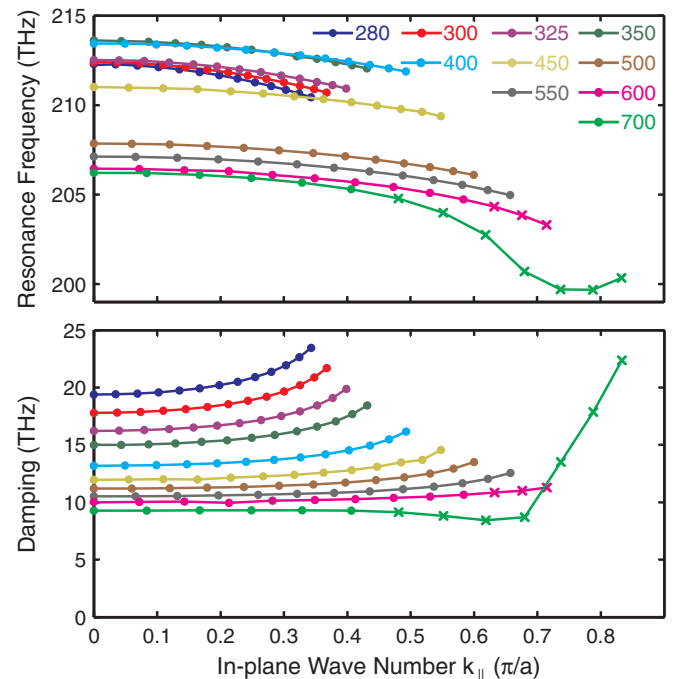

FIG. 9. (Color) As the experiment in Fig. 4, but derived from complete numerical calculations for actual infinite gold split-ring-resonator square arrays with lattice constants a, as indicated. Note the good qualitative agreement with the experiment in Fig. 4. The lateral geometry of the split-ring resonators is indicated in Fig. 1. The gold film thickness is 40 nm, and the glass substrate is accounted for.

due to the proximity effect in electron-beam lithography) can strongly disturb the ordering of the different branches. After all, for example, a 5% SRR size variation translates into an absolute frequency variation of 10 THz at 200-THz center frequency. Hence a systematic increase of the lattice constant a leads to a systematic redshift of the center frequency Ω due to a decrease of the proximity effect. In contrast, the dispersion for a given branch and the entire behavior of the damping are not expected to sensitively depend on this aspect. In order to specifically identify the influence of long-range retarded interaction in SRR arrays, we performed the numerical calculations using fixed SRR dimensions for all lattice constants [see the inset in Fig. 1(a)].

Finally, it is interesting to ask why our[6] and other groups,[11,22] previous results on split-ring-resonator arrays could be described reasonably well by accounting for nearest-neighbor[6,11] or short-range[22] interactions only, whereas we conclude in the present paper that accounting for long-range interaction is mandatory. Broadly speaking, one simply must not conclude from the mere agreement between whatever model and experiment that the model is correct. One can only conclude consistency. Agreement is a necessary but not a sufficient condition. More specifically, if we had not investigated the angle dependence (as, e.g., Refs. 7,8,10, and 11), i.e., if we would have had only data points at $k_{||} = 0$ for our discussion, our data were also compatible with the assumption of nearest-neighbor interaction only. In other words, the fact that we have measured simultaneously the dependence of the resonance frequency and of the damping on lattice constant as well as the dependence on angle of incidence (equivalent to in-plane wave vector) has provided a much more stringent test ground for a detailed understanding of split-ring-resonator arrays.

VI. CONCLUSION

In conclusion, we have provided a detailed experimental study of the resonance damping of split-ring-resonator square arrays. We find a characteristic dependence of the damping on lattice constant and on in-plane wave vector that is interpreted in terms of a retarded and long-range interaction among the split-ring resonators. This interpretation is backed up by three different levels of theoretical modeling.

These overall results imply that the damping in optical metamaterials can be fine tuned by suitably arranging the individual meta-atoms with respect to each other. The long-range interaction is also quite relevant in the context of the lasing spaser.[23–25] Without interaction, a large array of split-ring resonators would very likely break up into incoherent domains, whereas sufficiently strong long-range interaction could force the entire array into a collective coherent lasing-spasing mode.

[1]J. B. Pendry, A. J. Holden, D. J. Robbins, and W. J. Stewart, IEEE Trans. Microwave Theory Tech. **47**, 2075 (1999).

[2]D. R. Smith, W. J. Padilla, D. C. Vier, S. C. Nemat-Nasser, and S. Schultz, Phys. Rev. Lett. **84**, 4184 (2000).

[3]S. Linden, C. Enkrich, M. Wegener, J. Zhou, T. Koschny, and C. M. Soukoulis, Science **306**, 1351 (2004).

[4]C. M. Soukoulis, S. Linden, and M. Wegener, Science **315**, 47 (2007).

[5]L. Solymar, E. Shamonina, and L. Solymar, *Waves in Metamaterials* (Oxford University Press, Oxford, UK, 2009).

[6]M. Decker, S. Burger, S. Linden, and M. Wegener, Phys. Rev. B **80**, 193102 (2009).

[7]S. A. Maier, M. L. Brongersma, P. G. Kik, and H. A. Atwater, Phys. Rev. B **65**, 193408 (2002).

[8]C. Dahmen, B. Schmidt, and G. von Plessen, Nano Lett. **7**, 318 (2007).

[9]A. F. Koenderink, R. de Waele, J. C. Prangsma, and A. Polman, Phys. Rev. B **76**, 201403 (2007).

[10]P. Olk, J. Renger, M. T. Wenzel, and L. M. Eng, Nano Lett. **8**, 1174 (2008).

[11]I. Sersic, M. Frimmer, E. Verhagen, and A. F. Koenderink, Phys. Rev. Lett. **103**, 213902 (2009).

[12]N. Liu, H. Guo, L. Fu, S. Kaiser, H. Schweizer, and H. Giessen, Nat. Mater. **7**, 31 (2007).

[13]M. Decker, M. Ruther, C. E. Kriegler, J. Zhou, C. M. Soukoulis, S. Linden, and M. Wegener, Opt. Lett. **34**, 2501 (2009).

[14]M. Decker, R. Zhao, C. M. Soukoulis, S. Linden, and M. Wegener, Opt. Lett. **35**, 1593 (2010).

[15]J. K. Gansel, M. Thiel, M. S. Rill, M. Decker, K. Bade, V. Saile, G. von Freymann, S. Linden, and M. Wegener, Science **325**, 1513 (2009).

[16]C. Enkrich, M. Wegener, S. Linden, S. Burger, L. Zschiedrich, F. Schmidt, J. F. Zhou, T. Koschny, and C. M. Soukoulis, Phys. Rev. Lett. **95**, 203901 (2005).

[17]R. Marques, J. D. Baena, M. Beruete, F. Falcone, T. Lopetegi, M. Sorolla, F. Martin, and J. Garcia, J. Opt. A **7**, 38 (2005).

[18]M. Beruete, M. Sorolla, R. Marques, J. D. Baena, and M. Freire, Electromagnetics **26**, 247 (2006).

[19]F. Hesmer, E. Tatartschuk, O. Zhuromskyy, A. A. Radkovskaya, M. Shamonin, T. Hao, C. J. Stevens, G. Faulkner, D. J. Edwards, and E. Shamonina, Phys. Status Solidi B **244**, 1170 (2007).

[20]E. M. Purcell and C. R. Pennypacker, Astrophys. J. **186**, 705 (1973).

[21]B. T. Draine, Astrophys. J. **333**, 848 (1988).

[22]E. Shamonina, V. A. Kalinin, and L. Solymar, Electron. Lett. **38**, 371 (2002).

[23]D. J. Bergman and M. I. Stockman, Phys. Rev. Lett. **90**, 027402 (2003).

[24]M. I. Stockman, Nat. Photon. **2**, 327 (2008).

[25]N. I. Zheludev, S. L. Prosvirnin, N. Papasimakis, and V. A. Fedotov, Nat. Photon. **2**, 351 (2008).